Mon. Not. R. Astron. Soc. **000**, 1–**??** (2010) Printed 25 March 2010 (MN LATEX style file v2.2)

arXiv:1003.3669v2 [astro-ph.CO] 24 Mar 2010

Galaxy group at z=0.3 associated with the damped Lyman alpha system towards quasar Q1127–145

Glenn G. Kacprzak,[1]★ Michael T. Murphy,[1] and Christopher W. Churchill[2]
[1] *Centre for Astrophysics and Supercomputing, Swinburne University of Technology, PO Box 218, Victoria 3122, Australia*
[2] *Department of Astronomy, New Mexico State University, Las Cruces, NM 88003*

December 14 2009

ABSTRACT

We performed a spectroscopic galaxy survey, complete to $m_{F814W}\leqslant 20.3$ ($L_B > 0.15L_B^\star$ at $z = 0.3$), within 100×100″ of the quasar Q1127–145 ($z_{em} = 1.18$). The VLT/UVES quasar spectrum contains three $z_{abs}<0.33$ Mg ii absorption systems. We obtained eight new galaxy redshifts, adding to the four previously known, and galaxy star formation rates (SFRs) and metallicities were computed where possible. A strong Mg ii system [$W_r(2796) = 1.8$ Å], which is a known damped Lyα absorber (DLA), had three previously identified galaxies; we found two additional galaxies associated with this system. These five galaxies form a group with diverse properties, such as a luminosity range of $0.04 \leqslant L_B \leqslant 0.63L_B^\star$, an impact parameter range of $17 \leqslant D \leqslant 241$ kpc and velocity dispersion of $\sigma = 115$ km s^{-1}. The DLA group galaxy redshifts span beyond the 350 km s^{-1} velocity spread of the metallic absorption lines of the DLA itself. The two brightest group galaxies have SFRs of ∼few $M_\odot$ yr^{-1} and should not have strong winds. We have sufficient spectroscopic information to directly compare three of the five group galaxies' (emission-line) metallicities with the DLA (absorption) metallicity: the DLA metallicity is 1/10th solar, substantially lower than the three galaxies' which range between less than 1/2 solar to solar metallicity. HST/WFPC–2 imaging shows perturbed morphologies for the three brightest group galaxies, with tidal tails extending ∼25 kpc. We favor a scenario where the DLA absorption originates from tidal debris in the group environment.

Another absorber exhibits weak Mg ii absorption [$W_r(2796) = 0.03$ Å] and had a previously identified galaxy at a similar redshift. We have identified a second galaxy associated with this system. Both galaxies have solar metallicities and unperturbed morphologies in the HST/WFPC–2 image. The SFR of one galaxy is much lower than expected for strong outflows. Finally, we have also identified five galaxies at large impact parameters with no associated Mg ii absorption [$W_r(2796) \lesssim 5.7$ mÅ, 3 σ] in the spectrum of Q1127–145.

Key words: —galaxies: ISM, haloes, interactions —quasars: absorption lines.

1 INTRODUCTION

Absorption lines detected in the spectra of background quasars and gamma ray bursts remain one of the best probes of intervening multiphase gas throughout the Universe. Pioneering work of Bergeron (1988) and Bergeron & Boissé (1991) led to the first galaxies identified in close proximity to a quasar sight-line and at the same redshift as metal-enriched absorption traced by the Mg ii $\lambda\lambda 2796, 2803$ doublet. Since then, there has been numerous studies of Mg ii absorption line systems aimed at interpreting the properties of galaxy halos at a variety of redshifts (e.g., Le Brun et al. 1993; Steidel, Dickinson, & Persson 1994; Churchill, Steidel, & Vogt 1996; Churchill et al. 2000b; Steidel et al. 2002; Ellison et al. 2003; Bouché et al. 2006; Zibetti et al. 2007; Kacprzak et al. 2008; Chen & Tinker 2008; Barton & Cooke 2009; Rubin et al. 2009a; Pollack et al. 2009; Ménard et al. 2009).

Mg ii absorption lines are ideal for studying a large dynamic range of structures and environments in and around galaxies since they trace low ionization metal-enriched gas with neutral hydrogen column densities of $10^{16} \lesssim$ N(H i) $\lesssim 10^{22}$ cm^{-2}(Churchill et al. 2000a; Rigby, Charlton, & Churchill 2002). This large density range allows for detections of Mg ii in absorption out to ∼ 120 kpc from the host galaxy (Zibetti et al. 2007; Chen & Tinker 2008; Kacprzak et al. 2008).

Significant theoretical efforts have employed semi-analytical models and single halo galaxy simulations to interpret and understand absorption systems (e.g., Mo & Miralda-Escude 1996; Burkert & Lin 2000; Lin & Murray 2000; Maller & Bullock 2004; Chelouche et al. 2008; Chen & Tinker 2008; Tinker & Chen 2008;

★ gkacprzak@astro.swin.edu.au

Kaufmann et al. 2009). These models and simulations have helped constrain halo sizes, covering fractions, gas kinematics, physical gas conditions, etc. However, the majority of these studies modeled galaxies as isolated systems/halos and lack the important dynamic influences of the cosmic structure and local environments, which also may contribute to a significant fraction of the detected Mg II absorption (Kacprzak et al. 2010).

Halo gas masses and cross sections are suggested to increase due to tidal streams produced by the interactions/minor mergers and/or increased star formation-induced winds caused by gas rich minor mergers (York et al. 1986; Rubin et al. 2009a). Mg II gas outflowing at ~ 500 km s^{-1} has been detected in winds of galaxies at $z \sim 1$ (e.g., Tremonti et al. 2007; Weiner et al. 2009; Rubin et al. 2009b). Winds have also been suggested to be responsible for high equivalent width Mg II absorbers (Bouché et al. 2006). Evidence of galaxy interactions producing Mg II absorption was discussed by Kacprzak et al. (2007) who reported a suggestive correlation between the Mg II rest equivalent width, $W_r(2796)$, and the galaxy morphological asymmetries normalized by impact parameter. They suggest that perturbations from minor galaxy mergers may be responsible for producing low equivalent width systems [$W_r(2796) <$ 1.5 Å]. These results are consistent with low redshift H I surveys where galaxies having a perturbed/warped disk, from a previous or ongoing minor merger, also have more extended H I disks/halos (Puche et al. 1992; Swaters, Sancisi & van der Hulst 1997; Rand 2000; Fraternali et al. 2002; Chynoweth et al. 2008; Sancisi et al. 2008). The aforementioned results suggest that galaxy environments may play a role in the metal enrichment of galaxy halos.

Lopez et al. (2008) performed the first statistical environmental study of absorption systems associated with 442 x-ray selected galaxy clusters (z =0.3–0.9) out to transverse distances of 2 h^{-1} Mpc. It was determined that galaxy clusters produce a factor of 15 over-abundance of strong equivalent width systems [$W_r(2796) > 2$ Å] compared to field galaxies. This over-abundance is higher in the centers of clusters than in the outer parts and also increases with cluster mass. In contrast, the dN/dz of weak Mg II systems [$W_r(2796) < 0.3$ Å] in clusters is consistent with those derived from environmentally unbiased samples. Lopez et al. (2008) argue that the detected over-abundance of strong systems is a result of the over-density of galaxies in a cluster region. The lack of an over-abundance of weak systems may imply they were destroyed by the cluster environment. Padilla et al. (2009) modeled these results and found environmental evidence of truncated Mg II halo sizes as a function of cluster radii. Their models require a median Mg II halo size of $r < 10$ h^{-1} kpc, compared to $35 - 85$ h^{-1} kpc for field galaxies, in order to reproduce the observed absorption-line statistics of Lopez et al. (2008). These x-ray selected clusters represent more extreme environments than in galaxy groups where the majority of galaxies reside. In x-ray clusters, ram-pressure stripping is an important environmental effect since the intracluster medium and galaxy velocities are much higher than in galaxy groups where ram-pressure stripping is negligible (Mulchaey & Zabludoff 1998). However, in groups the galaxy velocities are smaller and the interactions and mergers more frequent, resulting in increased gas covering fractions of the cool intragroup gas (Zabludoff & Mulchaey 1998).

A significant fraction of strong Mg II absorption systems are damped Lyman alpha systems (DLA) (Rao et al. 2003). Since the discovery of DLAs (Wolfe et al. 1986) their host galaxy properties and environments have remained largely unknown. Only a small fraction of DLA hosts have been identified and appear to be isolated galaxies in close proximity of the quasar LOS (Lacy et al. 2003; Møller et al. 2002; Rao et al. 2003; Chun et al. 2006). Models support an array of origins of the DLA absorbing gas from rotating thick disks (e.g., Prochaska & Wolfe 1997, 1998; Prochaska et al. 2002), gas rich dwarf galaxies (Matteucci et al. 1997), irregular protogalactic clumps (Haehnelt et al. 1998), and tidal gas or processes such as superwinds and outflows (Zwaan et al. 2008).

In this paper, we perform a spectroscopic survey of the galaxies in the Q1127−145 quasar field. A VLT/UVES quasar spectrum shows that there are three absorption systems in this field, one of which is DLA system which has three previously identified galaxies at a similar redshift. However, this field contains many unidentified bright galaxies within 50″ of the quasar line of sight. We perform a spectroscopic survey, to a limiting magnitude of $m_{F814W} \leqslant 20.3$, in an attempt to obtain spectroscopic redshifts for the remaining galaxies within the field. In § 2 we describe our sample and analysis. In § 3 we present the results of our redshift survey. We discuss morphologies of the galaxies and we also compute galaxy star formation rates (SFRs) and emission line metallicities when possible. We compare galaxy metallicities to the absorption line metallicity derived for the DLA. In § 4, we discuss the possible origins of the Mg II absorption and our concluding remarks are in § 5. Throughout we adopt an $\mathrm{H}_0 = 70$ km s^{-1}Mpc^{-1}, $\Omega_{\mathrm{M}} = 0.3$, $\Omega_\Lambda = 0.7$ cosmology.

2 TARGET FIELD AND OBSERVATIONS

Q1127−145 is a bright (V=16.9 mag) z_{em} =1.18, gigahertz-peaked radio source with a ~300 kpc jet seen in the x-ray and in multi-frequency radio observations (see Siemiginowska et al. 2002, 2007). A VLT/UVES spectrum of the quasar contains three Mg II absorption systems: z_{abs} =0.190973 (Evans et al., in prep), 0.312710 (Bergeron & Boissé 1991) and 0.328266 (Narayanan et al. 2007). To date, no galaxies have been found to have similar redshift as the z_{abs} =0.190973 Mg II absorption. One galaxy associated with the z_{abs} =0.328266 absorption system (labeled in this paper as G5) was recently spectroscopically confirmed by Kacprzak et al. (2010).

From a *HST*/FOS UV spectrum, the z_{abs} =0.312710 was determined to be a DLA with $N_{HI} = 5.1 \pm 0.9 \times 10^{21}$ cm^{-2} (Rao & Turnshek 2000). Bergeron & Boissé (1991) spectroscopically identified two galaxies (labeled in this paper as G2 and G4) to be at a similar redshift as the z_{abs} =0.312710 absorption system. Since G2 is closer to the quasar line of sight (LOS) and has more significant star formation than G4, G2 was favored as the absorbing galaxy. Lane et al. (1998) later obtained a spectroscopic redshift of another galaxy, called G1 here, which is also consistent with the absorption redshift and was then favored as the absorbing galaxy due to its closer proximity to the quasar LOS than G2 and G4. Additional multi-band imaging studies claim to have detected low surface brightness emission around the quasar and also a possible underlying galaxy 0.6″ from the quasar LOS (Nestor et al. 2002; Rao et al. 2003; Chun et al. 2006). However, it is possible that the low surface brightness signal is coming from radio-loud/x–ray emitting quasar host galaxy at $z_{em} = 1.18$ (Siemiginowska et al. 2002, 2007). In either case, this field does not contain the typical isolated galaxy and absorber seen in many quasar absorber fields. (e.g., Steidel, Dickinson, & Persson 1994; Steidel et al. 1997; Guillemin & Bergeron 1997).

The Q1127−145 field appears to have an unusually large number of bright galaxies within 100″×100″ centered on the quasar line of sight. Here we have performed a shallow spectroscopic survey

Table 1. Summary of the galaxy spectroscopic observations obtained with the ARC 3.5m using the double imaging spectrograph (DIS). Four different DIS long-slit positions were obtained and their spatial are shown in Figure 1. The instrument gratings and central wavelengths (λ_c) were selected to target Hα and [N II] emission lines, on the red channel, and [O II] emission lines, on the blue channel, for $z \sim 0.3$ galaxies.

Slit Position	Grating	λ_c (Å)	Date (UT)	Exposure (seconds)
Slit 1	B1200	4500	2008 Jan. 16	10,500
	R1200	7300	2008 Jan. 16	4500
	R1200	8500	2008 Jan. 16	6000
Slit 2	B1200	5220	2008 Feb. 01	4500
	R830	9040	2008 Feb. 01	4500
Slit 3	B1200	4700	2008 Feb. 01	3000
	B1200	5220	2008 Mar. 27	6000
	R830	9040	2008 Feb. 01	3000
	R830	9040	2008 Mar. 27	6000
Slit 4	B1200	5220	2008 Feb. 01	3000
	R830	9040	2008 Feb. 01	3000

of the field at a limiting magnitude of $m_{F814W} \leqslant 20.3$ in an attempt to identify the remaining absorbing galaxies within the field. At the redshift of the DLA the $B-$band luminosity limit is $L_B = 0.15 L_B^{\star}$.

2.1 Galaxy Spectroscopy

Galaxy spectra were obtained during three nights between 2008 January and 2008 March using the double imaging spectrograph (DIS) at the Apache Point Observatory (APO) 3.5m telescope in New Mexico. Details of the observations are presented in Table 1. The spectrograph has separate red and blue channels that have plate scales of 0.40″ pixel^{-1} and 0.42″ pixel^{-1}, respectively. We used a 1.5″-wide by 6′-long slit with no on-chip binning of the CCD.

The B1200 grating was used for the blue channel resulting in a spectral resolution of 0.62 Å pixel^{-1} with wavelength coverage of 1240 Å. For the red channel, both the R830 and the R1200 gratings were used. The R830 grating has a spectral resolution of 0.84 Å pixel^{-1} with wavelength coverage of 1680 Å. The R1200 has a spectral resolution of 0.58 Å pixel^{-1} with wavelength coverage of 1160 Å. Wavelength centers for each grating (see Table 1) were selected to target [O II], Hα, and [N II] emission lines for $z \sim 0.3$ galaxies. The total exposure time per target ranges from 3000 to 10,500 seconds and the observations were performed during poor/cloudy weather conditions with typical seeing of 1–2″. Four slit positions were obtained and are shown in Figure 1.

Spectra were reduced using IRAF[1]. External quartz dome-illuminated flat fields were used to eliminate pixel-to-pixel sensitivity variations. Stellar spectra taken in the same field were used as traces to facilitate the extraction of the faint galaxy spectra. Each spectrum was wavelength calibrated using HeNeAr arc line lamps. The galaxy spectra were both vacuum and heliocentric velocity corrected.

A Gaussian fitting algorithm (see Churchill et al. 2000a), which computes best fit Gaussian amplitudes, centers, and widths, was used to obtain the galaxy redshifts from one or more emission lines. Emission lines used to calculate the galaxy redshift were detected at or above the 3 σ level (the galaxy redshifts are listed in Table 3).

Table 2. Summary of the imaging observations of the Q1127–145 field obtained using *HST* with the WFPC–2. The images were taken with the F814W filter with the quasar centered on chip 3 of the CCD array. The images were taken at a range of position angles (PA) listed below. In column 6 we list the Proposal IDentification number (PID) of the WFPC–2 observations taken by the PI Bechtold.

Filter	Quasar Location	Chip PA	Exposure (seconds)	Date	PID
F814W	WF3	−11.502	4400	May 23 2001	9173
F814W	WF3	−3.102	4400	Aug. 01 2001	9173
F814W	WF3	147.006	4400	Nov. 16 2001	9173
F814W	WF3	147.863	4400	Nov. 16 2001	9173
F814W	WF3	164.698	4400	Jan. 03 2002	9173

Higher resolution spectra of three previously identified galaxies (G2, G4, and G5) were obtained by Kacprzak et al. (2010). Their Keck/ESI spectra have a velocity resolution of 11 km s^{-1} pixel^{-1} and have a range of exposure times of 600–4200 seconds. Details regarding the individual spectra and the data reductions are presented in Kacprzak et al. (2010). Here we present the flux calibrated spectra for these three galaxies. The spectra were calibrated using IRAF with standard stars taken during the night of the observation. We have made no corrections for slit loss nor reddening.

2.2 Quasar Spectroscopy

The absorption properties were measured from VLT/UVES (Dekker et al. 2000) archival spectra of Q1127−145 obtained on 2002 August 17 [PI Lane, PID 67.A-0567(A)], 2003 August 18 [PI Savaglio, PID 69.A-0371(A)], and 2007 May 3 [PI Miniati, PID 076.A-0860(A)]. The UVES spectrum has a wavelength coverage from 3046–4517 Å and from 4622–6810 Å. All spectra were taken with 2 × 2 binning using a 1″-wide slit, providing a spectral resolution with FWHM 7 km s^{-1}. They were reduced using the standard ESO pipeline and the custom code UVES Post–Pipeline Echelle Reduction (UVES POPLER[2]). The spectrum is both vacuum and heliocentric velocity corrected. Analysis of the Mg II absorption profiles was performed using interactive software (see Churchill et al. 1999, 2000a; Churchill & Vogt 2001) for local continuum fitting, objective feature identification, and measuring absorption properties. The absorption redshifts are computed from the optical depth weighted mean of the Mg II absorption profile (see Churchill & Vogt 2001). The typical absorption redshift uncertainty is ∼ 0.3 km s^{-1}. Velocity widths of absorption systems are measured between the pixels where the equivalent width per resolution element recovers to the 1 σ detection threshold (Churchill et al. 1999).

---

[1] IRAF is written and supported by the IRAF programming group at the National Optical Astronomy Observatories (NOAO) in Tucson, Arizona. NOAO is operated by the Association of Universities for Research in Astronomy (AURA), Inc. under cooperative agreement with the National Science Foundation.

[2] http://astronomy.swin.edu.au/∼mmurphy/UVES_popler.html

Table 3. Galaxy-absorber sample towards Q1127−145. The table columns are (1) the galaxy ID as referenced in the text and figures, (2) the galaxy angular separation from the quasar line of sight, θ, (3) the galaxy redshift, (4) the reference(s) for the galaxy spectroscopic identification, (5) the quasar-galaxy impact parameter, D, (6) the galaxy apparent magnitude, (7) the absolute B-band magnitude with its B-band luminosity (8), (9) the galaxy group ID, (10) Mg II absorption redshift, (11) the rest-frame Mg II λ2796 equivalent width, W_r(2796), and (12) the galaxy velocity offsets from the optical depth weighted mean Mg II absorption. Note that we find a group of at least five galaxies at similar redshifts as the DLA system ($z_{abs} = 0.312710$) and two galaxies at similar redshifts to the weak Mg II absorption system at $z_{abs} = 0.328266$. We also find five non-absorbing galaxies.

ID	θ ($''$)	z_{gal}	REF[a]	D (kpc)	m_{F814W}	M_B	L_B ($L_B^\star$)	Group ID	z_{abs}	W$_r$(2796)[b] (Å)	Δv_r[c] (km s^{-1})
G1	3.81	0.3121±0.0003	1	17.4±0.1	21.55±0.37	−17.7	0.04	1	0.312710	1.773±0.006	+140
G2	10.01	0.3132±0.0002	2,3,4	45.6±0.3	18.81±0.11	−20.4	0.54	1	0.312710	1.773±0.006	−112
G3	16.23	0.32839±0.00003	5	76.9±0.4	20.12±0.20	−19.2	0.18	2	0.328266	0.029±0.003	−28
G4	17.77	0.3124±0.0001	2,3,4	81.0±0.3	18.64±0.10	−20.6	0.63	1	0.312710	1.773±0.006	+71
G5	19.30	0.32847±0.00003	4	91.4±0.2	18.84±0.11	−20.5	0.60	2	0.328266	0.029±0.003	−46
G6	21.76	0.31167±0.00003	5	99.8±0.1	19.79±0.17	−19.4	0.22	1	0.312710	1.773±0.006	+238
G7	27.92	0.27921±0.00007	5	118.3±0.8	20.22±0.21	−18.7	0.11	···	···	<0.0049	···
G8	33.22	···[d]	···	···	20.08±0.19	···	···	···	···	···	···
G9	33.91	0.20735±0.00006	5	115.2±0.2	19.85±0.19	−18.3	0.08	···	···	<0.0050	···
G10	37.93	···[d]	···	···	19.94±0.19	···	···	···	···	···	···
G11	38.12	0.33293±0.00002	5	182.3±0.2	19.76±0.17	−19.6	0.27	···	···	<0.0048	···
G12	43.23	0.30515±0.0004	5	195.0±0.6	19.50±0.15	−19.65	0.27	···	···	<0.0048	···
G13	50.08	···	···	···	20.14±0.20	···	···	···	···	···	···
G14	52.54	0.31243±0.00003	5	240.8±0.3	20.01±0.19	−19.2	0.18	1	0.312710	1.773±0.006	+64
G15	68.22	0.2473±0.0002	5	264.8±0.3	19.00±0.12	−19.6	0.25	···	···	<0.0057	···

[a] Galaxy Identification: (1) Lane et al. (1998), (2) Bergeron & Boissé (1991), (3) Guillemin & Bergeron (1997), (4) Kacprzak et al. (2010), (5) This work.
[b] Equivalent width limits are 3σ. [c] Δv_r is the rest-frame velocity offset between the mean Mg II λ2976 absorption line and the galaxy where, $\Delta v_r = c(z_{abs} - z_{gal})/(1 + z_{gal})$ km s^{-1}. [d] No strong emission lines were detected.

2.3 HST Imaging

The WFPC–2/*HST* F814W images were obtained from the Hubble Legacy Archive (HLA[3]) (PI Bechtold). Details of the WFPC–2/*HST* observations are presented in Table 2. Five sets of four 1100s exposures were taken over a range of position angles. In all of the images, the quasar was positioned in the center of chip 3 of the WFPC–2 camera. We combined the five 4400s images using IRAF IMCOMBINE.

Galaxy photometry was performed using the Source Extractor (SExtractor) package (Bertin & Arnouts 1996) with a detection criterion of 1.5 σ above background. The m_{F814W} magnitudes were computed using the WFPC–2 zero points taken from Table 5.1 of the WFPC–2 Data Handbook and the chip gains obtained from the WFPC–2 Instrument Handbook. All magnitudes are based upon the Vega system.

Galaxy absolute B-band magnitudes, M_B, were determined from the k–corrected observed m_{F814W}. The k–corrections were computed using the formalism of Kim, Goobar, & Perlmutter (1996) using the spectral energy distribution (SED) templates of Kinney et al. (1996). We adopted a Sb SED which is consistent with the average colour of Mg II absorbing galaxies (Steidel, Dickinson, & Persson 1994; Zibetti et al. 2007). B–band luminosities were computed using the DEEP2 optimal $M_B^\star$ of Faber et al. (2007, Table 2) in the redshift bin appropriate for each galaxy ($M_B^\star = -21.07$ for $\langle z \rangle = 0.3$).

3 RESULTS

Here we discuss the galaxies identified in our redshift survey along with galaxies identified in previous works. In Figure 1 we present a 100×100$''$ portion of the combined WFPC2 image centered on the quasar. The four slit positions used in our new observations are indicated on the image. In Table 3, we list all the galaxies in the quasar field that have $m_{F814W} < 20.3$ within $100 \times 100''$ box centered on the quasar (we have included galaxy G1 since it has a spectroscopic redshift and G15 which is beyond the surveyed region).

We have obtained spectroscopic redshifts for eight new galaxies in this work. We have identified: (1) a group of galaxies associated with the DLA, (2) a pair of galaxies associated with a weak Mg II absorption system, and (3) five non-absorbing galaxies. The offsets of the systemic velocity of the absorbing galaxies from the optical depth weighted mean Mg II absorption are also listed in Table 3 and range from −112 to +238 km s^{-1}. In the following subsections we will discuss the galaxies identified in the Q1127−145 field.

3.1 Non-Absorbing Galaxies

We have spectroscopically confirmed the redshifts of five non-absorbing galaxies for which we do not detect Mg II absorption to the limits of the UVES spectrum. In Figure 2 we show 10$''$×10$''$ images of these galaxies along with their emission line spectra. Galaxies are listed in increasing impact parameter order. The galaxy redshifts were determined using Hα and/or [O II] emission lines. From the *HST* image, the non-absorbing galaxies appear to be normal spiral disks and the spectra indicate they have ongoing star formation.

Three galaxies (G7, G12, and G15) have been spectroscopically confirmed with two emission lines while two galaxies (G9 and G11) have been confirmed with a single line. There is the possibility that the redshifts of galaxies computed with only one emission line may be incorrect. However, given the wavelengths of these lines and the observed apparent magnitudes of the galaxies, it is highly unlikely that these are at different redshifts than the

---

[3] http://hla.stsci.edu/

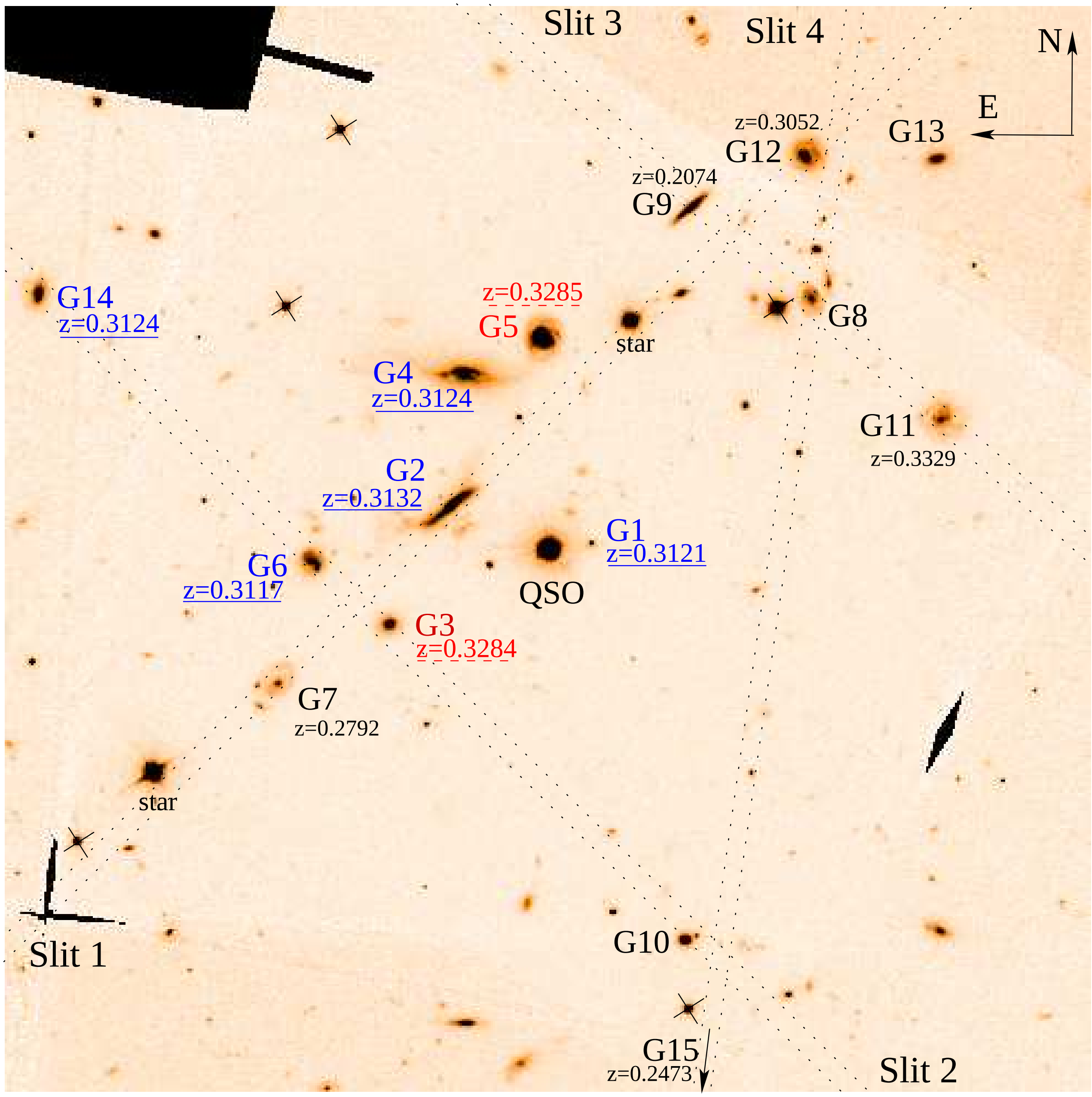

Figure 1. 100″ × 100″ *HST*/WFPC–2 F814W image of the quasar field Q1127−145. The quasar is located in the center of the image. Black regions have no WFPC–2 coverage. The four slit positions are indicated with dotted lines. All galaxies with spectroscopically confirmed redshifts are indicated. The galaxy redshifts are only quoted to four significant figures for clarity (see Table 3 for full redshifts). Galaxy G15, an image of which can be found in Figure 5, is beyond the 100″ × 100″ image shown here. Note there are two distinct groupings of galaxies – one at $z \sim 0.313$ (blue/solid line) and at $z \sim 0.328$ (red/dashed line) – and the former is the galaxy group associated with the DLA at $z_{abs} = 0.313$. Point source objects, which are likely stars, are indicated with an "X". Objects that have been spectroscopically identified as stars are indicated.

ones quoted here. The redshift of G9 was computed using the [O ii] emission line and is reliable because since the observed [O ii] wavelength is ∼ 4503 Å, which is bluer than any other optical galaxy emission line rest wavelength and is not likely to be a UV emission line since it would place the galaxy at a redshift $z > 2$. The redshifts of G11 and G14 were computed using only the Hα emission line. If the Hα emission line is incorrectly identified then the next likely candidate line would be [O iii]. This would place the galaxy at redshifts of $z > 0.7$, which would result in $L_B \geqslant 1.5L_B^*$ with a disk scale length $\geqslant$ 4.5 kpc. We are therefore confident in these emission line identifications.

All non-absorbing galaxies have Mg ii equivalent width 3σ detection limits of 4.8−5.7 mÅ (see Table 3). These equivalent width limits are quite low and imply that these galaxies are not associated with any substantial Mg ii absorption along the LOS, which can be interpreted as either the quasar LOS passing outside the galaxies' Mg ii enriched halos or through a void within the patchy Mg ii halo gas distribution. It is important to note that all the non-absorbing galaxies have impact parameters $D > 118$ kpc. This is consistent

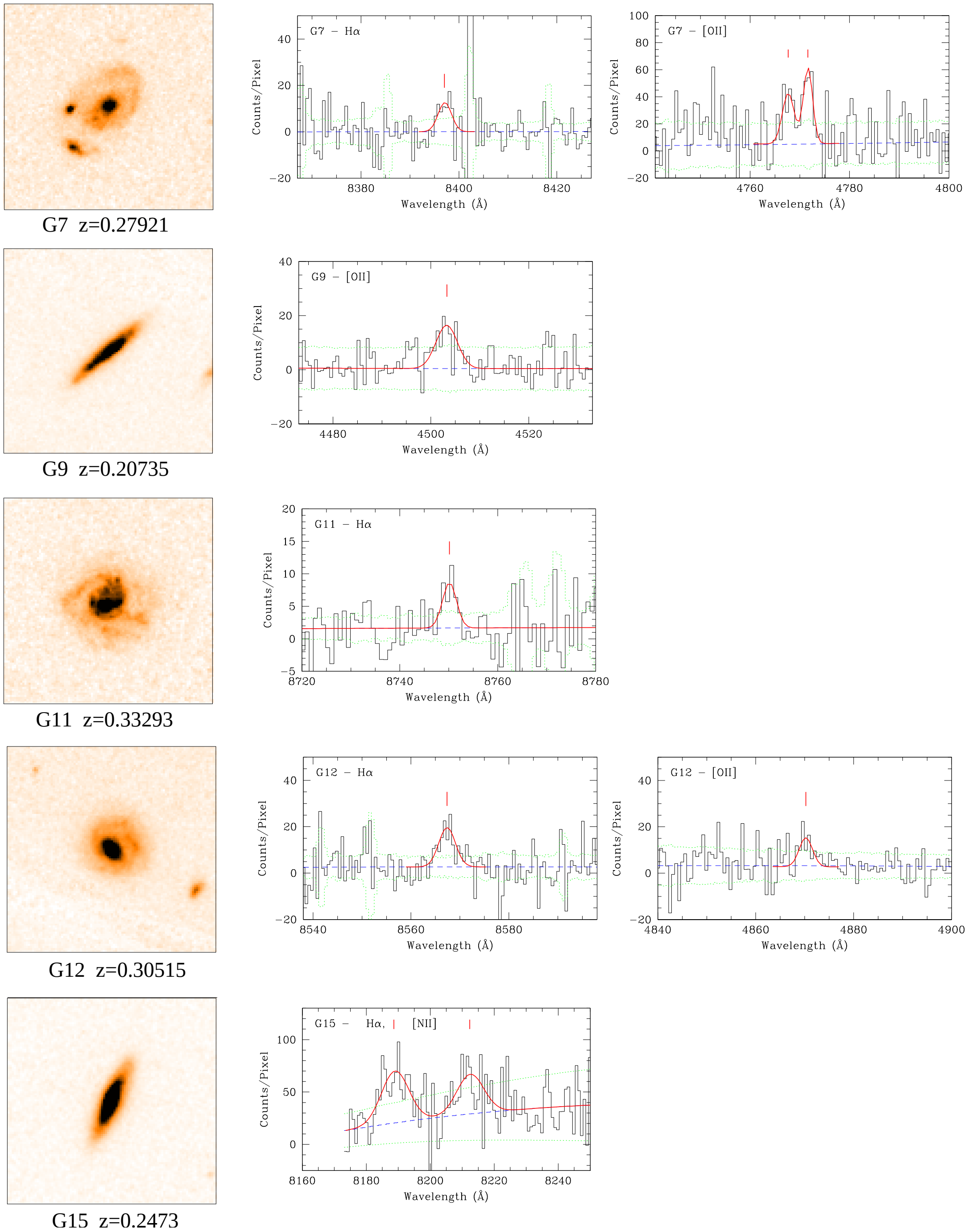

Figure 2. 10 × 10″ WFPC–2 F814W images of the non-absorbing galaxies G7 (image size 42.4 × 42.4 kpc), G9 (34.0 × 34.0 kpc), G11 (47.8 × 47.8 kpc), G12 (45.1 × 45.1 kpc), and G15 (38.8 × 38.8 kpc). The galaxies are shown in increasing impact parameter order and have the same orientation as in Figure 1. The Hα and/or [O II] galaxy emission lines used to spectroscopically confirm the galaxy redshift are shown. Three galaxies (G7, G12, and G15) have been identified using two emission lines while two galaxies (G9 and G11) have been identified with one. The blue dashed lines are the fits to the continuum and the solid red curves are fits to the data. The green dotted lines are the 3σ detection limits.

with current studies that show most luminous galaxies at projected distances within D ∼120 kpc are Mg II absorbers while beyond D ⩾120 kpc they are not (Churchill, Kacprzak, & Steidel 2005; Zibetti et al. 2007; Kacprzak et al. 2008; Chen & Tinker 2008).

3.2 $z_{abs} = 0.328$ Galaxies

We have spectroscopically confirmed one new galaxy (G3) at $z = 0.328$ in addition to G5, which was spectroscopically identified by Kacprzak et al. (2010). Both galaxies have strong Hα and N II emission lines shown in Figure 3. G3 has the smallest impact parameter of $D = 76.9$ kpc and has a Hα rest equivalent width of 32.0 Å. G5 has an impact parameter of $D = 91.4$ kpc and has a Hα rest

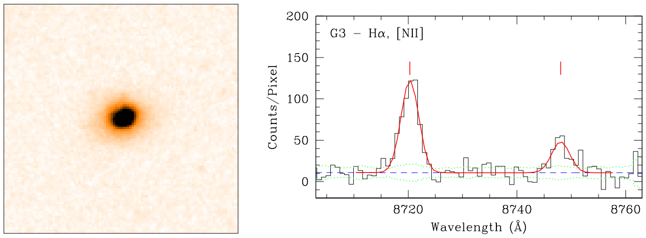

G3 z=0.32839

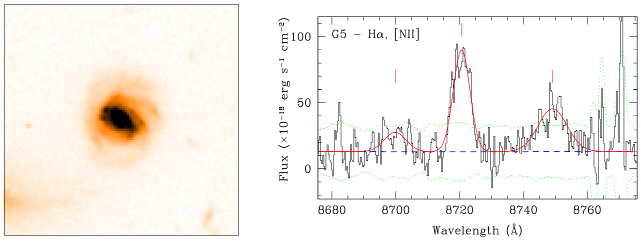

G5 z=0.32847

Figure 3. Same as Figure 2 except for the two galaxies G3 and G5 associated with the $z = 0.328$ absorption system. The spectrum of G5 was obtained with Keck/ESI and is flux calibrated. The images are 47.4×47.4 kpc in size at the redshift of the absorption.

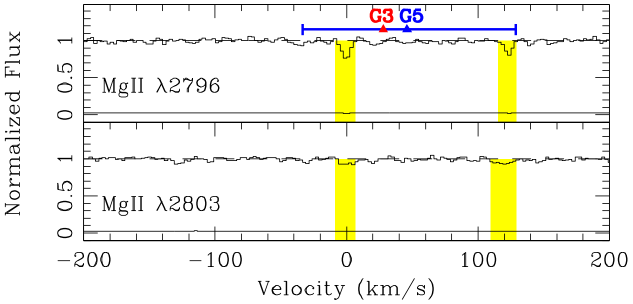

Figure 4. The observed Mg ii $\lambda\lambda$2796, 2803 absorption in the UVES quasar spectrum at velocities relative to z_{abs} =0.328266. The dashed line is a fit to the continuum and the solid line near zero is the flux error spectrum. The Mg iiλ2796 absorption redshift is the zeropoint of the velocity scale and the absorption velocities are shaded in. The Mg iiλ2796 is detected to a significance level of 5 σ and the Mg iiλ2803 is detected to a significance level of 3 σ. The redshifts of both galaxies are indicated by the triangles and the maximum observed rotation velocities of G5, obtained from Kacprzak et al. (2010), are shown by the error bars. Note that if one includes the kinematics of both galaxies, they both have velocities consistent with the Mg ii absorption.

equivalent width of 29.5 Å. Both galaxies appear to have normal unperturbed morphology. G3 is a compact core $0.2L_B^\star$ galaxy with ongoing star formation while G9 is a $0.6L_B^\star$ galaxy with a large bar and a sizable bright bulge similar to a local SBb galaxy. The major differences between the two galaxies are that G9 is much brighter than G3 and exhibits spiral arms.

The z_{abs} = 0.328 Mg ii absorption was first reported by Narayanan et al. (2007), and is presented in Figure 4. This weak system is composed of two single clouds with a velocity separation of 124 km s^{-1} and has a total equivalent width of $W_r(2796)$ = 0.029 Å. No significant Mg i is detected (3σ, $W_r \leqslant 0.003$ Å). In Figure 4 we also show the galaxy systemic redshifts (triangles) relative to the absorption system. Note that both galaxies have redshifts that are bracketed with both absorption clouds.

Galaxy G5's rotation curve was obtained by Kacprzak et al. (2010) and the error bars in Figure 4 indicate its observed maximum rotation velocities. With a projected velocity span of ∼160 km s^{-1}, G5's dynamics is consistent with both absorption cloud velocities. In particular, Kacprzak et al. (2010) show that the two cloud velocities align with each side of the rotation curve, but that pure disk models are unable to reproduce the observed Mg ii absorption velocities. If we were able to obtain a rotation curve for G3, both galaxy kinematics would likely be consistent with both absorption clouds. Thus, in these circumstances, it is difficult to disentangle which galaxy is associated with this particular absorber. Yet associating the absorption with one galaxy or the other may result in a difference in conclusions regarding the origins of the absorption. We discuss the implications of this in Section 4.

3.3 z_{abs} = 0.313 Galaxies

Three previously spectroscopically confirmed galaxies associated with the DLA are G1, G2, and G4. G1 is the closest galaxy to the quasar line of sight having an impact parameter of D = 17.4 kpc. This faint $0.04L_B^\star$ compact core galaxy was identified from [O iii] emission lines (Lane et al. 1998). The next closest galaxy to the quasar line of sight is G2 with D = 45.6 kpc. This $0.54L_B^\star$ edge-on spiral displays asymmetries on both sides of the galaxy and its Hα rest equivalent width is 17.3 Å. The G4 galaxy has a major dust lane and a large bulge. Given that we detected no strong emission lines, this galaxy could either be classified as Sa or as an early-type S0 galaxy. It has a luminosity of $L_B = 0.63L_B^\star$ with impact parameter of D = 81.0 kpc.

We have spectroscopically confirmed two new galaxies (G6 and G14) at a similar redshift to the z_{abs} = 0.313 DLA in addition to the three previously discovered galaxies G1, G2, and G4 (Bergeron & Boissé 1991; Lane et al. 1998). All five galaxies are shown in increasing impact parameter order in Figure 5. The galaxy emission line strengths are shown in Table 4. The newly spectroscopically confirmed galaxy G6 has an impact parameter of D = 99.8 kpc and has a Hα rest equivalent width of 32.4 Å. This $0.22L_B^\star$ spiral galaxy has asymmetric spiral arms. G14 has an impact parameter of D = 240.8 kpc and has a Hα rest equivalent width 34.8 Å. This $0.18L_B^\star$ galaxy has a perturbed early-type morphology. Both newly identified galaxies are at larger impact parameters than the previously known ones (G1, G2 and G4), suggesting that the galaxy environment is more group-like and much larger than previously thought.

The galaxy group has five confirmed galaxies that have a luminosity range of $0.04 \leqslant L_B \leqslant 0.63L_B^\star$. The group of at least five galaxies has a velocity dispersion of σ = 115 km s^{-1} centered at a redshift of z_g = 0.31236.

The velocity spread of the galaxy group is comparable to the velocity spread of the Mg ii gas as seen in Figure 6. The galaxies cover a full velocity range of 350 km s^{-1}. The Mg ii absorption seems to occur in two separate kinematic components: the large, saturated component has a large velocity spread of 235 km s^{-1}, and the much weaker absorption bluewards of the saturated component comprises several clouds with a velocity spread of 68 km s^{-1}. The Mg ii absorption redshift is offset 80 km s^{-1} redward of the galaxy group redshift of z_g = 0.31236. In Figure 6, we show the rotation velocity ranges for G2 and G4 from Kacprzak et al. (2010). These galaxies are the brightest two in the group. The maximum observed projected rotational velocity for G2 is 204 km s^{-1} and G4 has maximum observed projected rotational velocity of 90 km s^{-1}.

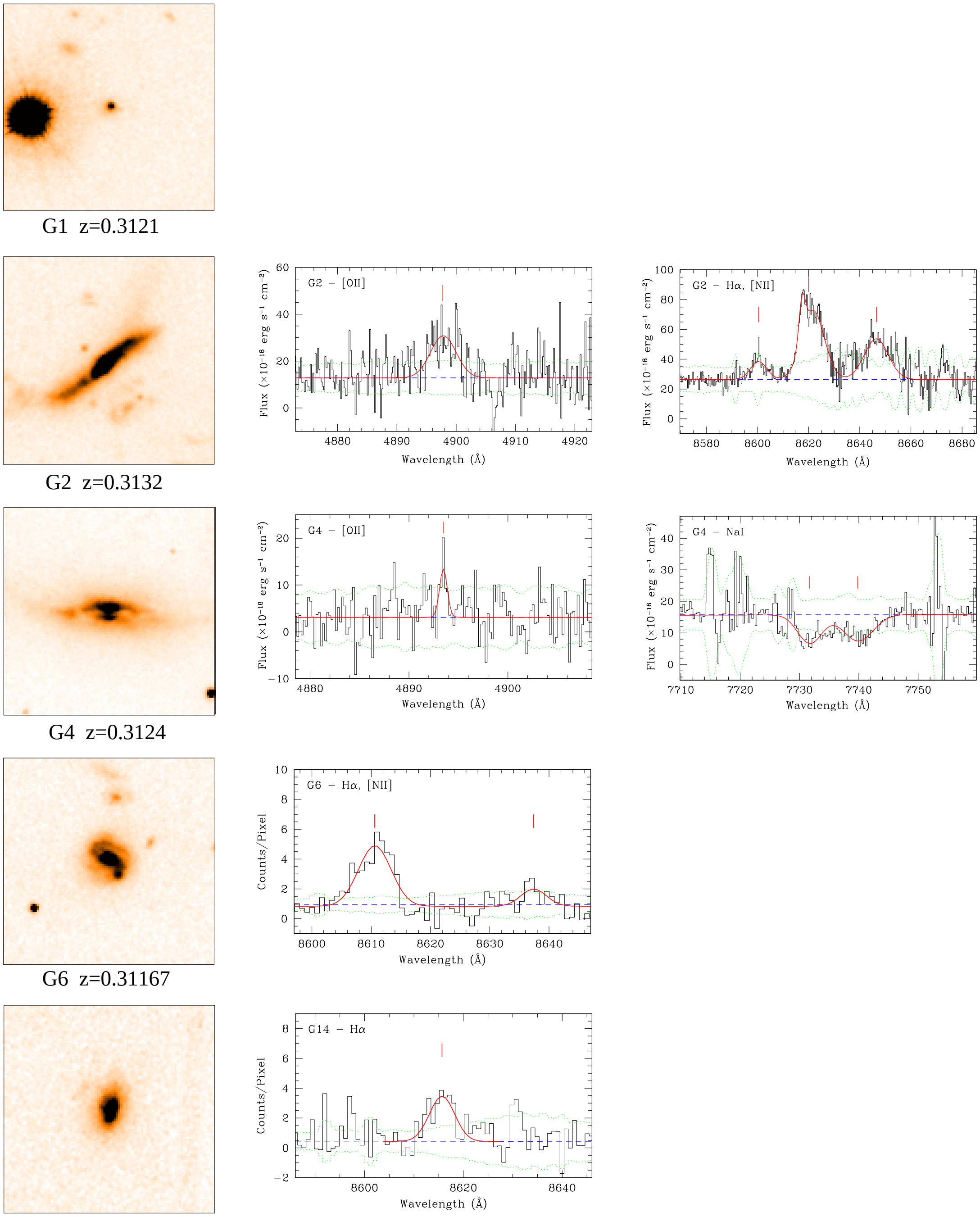

G1 z=0.3121

G2 z=0.3132

G4 z=0.3124

G6 z=0.31167

G14 z=0.31243

Figure 5. Same as Figure 2 except for the G1, G2, G4, G6, and G14 galaxy group associated with the z = 0.313 DLA. G1 was spectroscopically confirmed by Lane et al. (1998) and we do not have a spectrum of this galaxy to show here. The spectra of G2 and G4 were obtained with Keck/ESI and are flux calibrated. The images are 45.9×45.9 kpc in size at the redshift of the DLA absorption. For G4, we show the Na I absorption feature for reference since it was also used to confirm the redshift since the [O II] line is quite weak.

The rotation velocities of both G2 and G4 alone cover the full range of the absorption velocities. Kacprzak et al. (2010) note that, using a simple disk model, a large fraction of the absorption velocities could be explained by the halo gas of G2 and G4 rotating as thick disks. However, the disk model is quite unrealistic since it assumes the halo rotates at constant velocity, set by the maximum galaxy rotation velocity, independent of scale height. Therefore it is unlikely that all of the absorption is produced by co-rotating halo gas from both galaxies G2 and G4.

Using the Mg I profile, one can study the individual clouds that are saturated in Mg II. The majority of the Mg I gas is aligned with the saturated Mg II component. Only a very weak Mg I cloud is detected in a second kinematic component at −150 km s^{-1}. All detectable Fe II lines are highly saturated (see Figure 6). The absorption velocity structure is more apparent in the Ca II, Mn II and Ti II lines where five to six kinematically distinct absorption features are apparent. These features do not align with the five galaxy

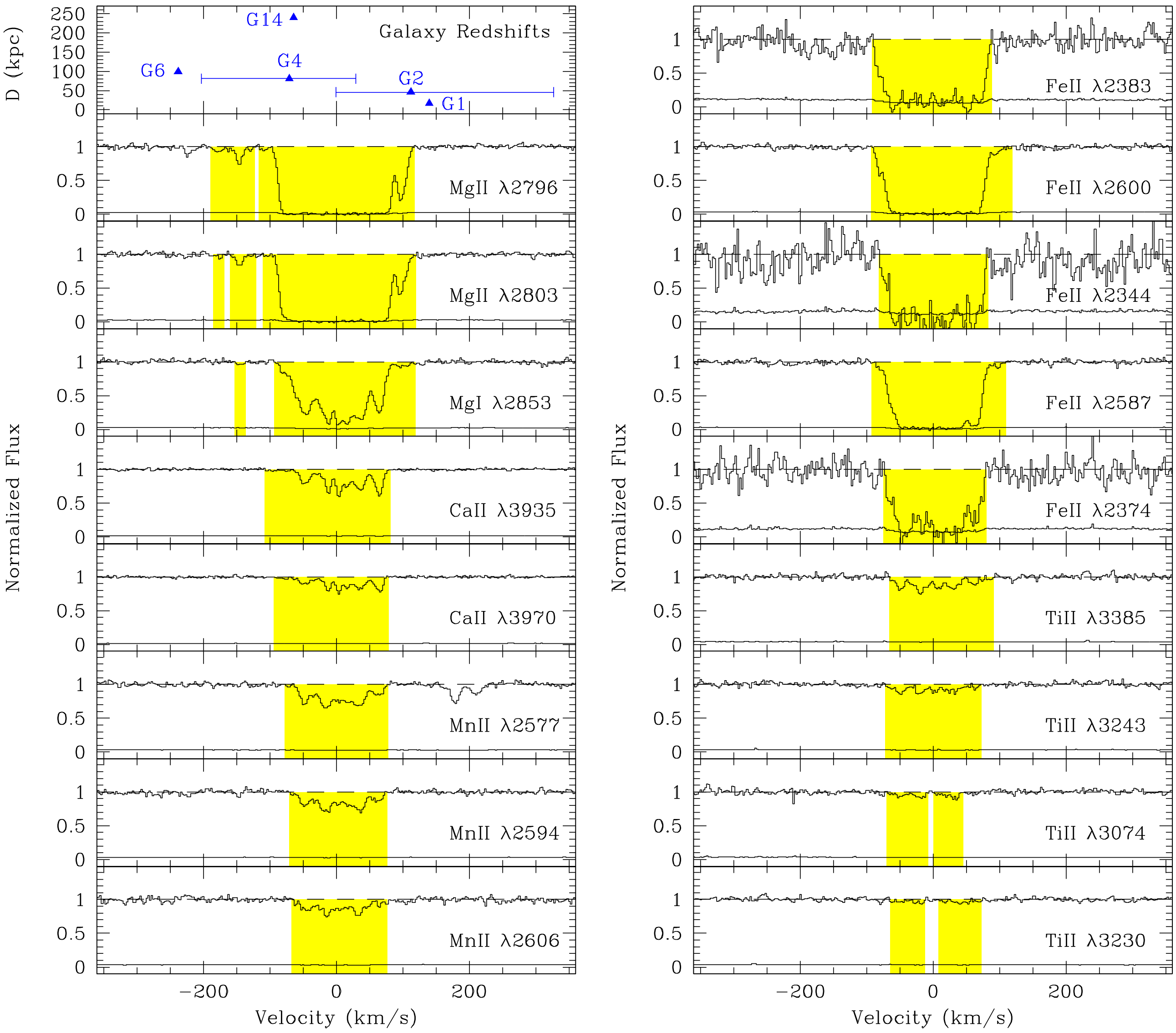

Figure 6. The observed metal-line absorption from the $z_{abs} = 0.313$ DLA obtained from the UVES quasar spectrum. The dashed line is a fit to the continuum and the solid line near zero is the flux error spectrum. The Mg iiλ2796 absorption redshift is the zeropoint of the velocity scale. The range of velocities over which significant absorption is detected are shaded for each transition; for Mg iiλ2796, the detection threshold was set at 5σ while a lower threshold of 3σ is set for all other transitions. The redshifts of all five galaxy group members are indicated by the triangles and are shown as a function of impact parameter. The maximum observed rotation velocities of G2 and G4 obtained from Kacprzak et al. (2010) are shown by the error bars. Note the redshift distribution of the galaxy group spans all of the absorption velocities. The observed rotational kinematics of G2 and G4 alone also span the absorption velocities.

redshifts in the group, making it difficult to determine the origin of the absorbing gas.

A *HST*/STIS E230M spectrum was also taken of this quasar (PI:Bechtold). The Zn ii present in the spectrum has the same velocity structure as the Ca ii and the measured Zn ii column density is 13.45 ± 0.08 cm^{-2}(Kanekar 2009, private communication). We discuss the metallicity of this DLA in greater detail in Section 3.5.

Lane et al. (1998) detected 21-cm absorption at a similar redshift to the DLA. Higher signal-to-noise and higher resolution 21-cm absorption spectra taken by Chengalur & Kanekar (2000) revealed that the broad feature detected by Lane et al. (1998) breaks up into a five to six narrow components. The full velocity width of the absorption is ~ 120 km s^{-1}, which is comparable to the velocity widths of the Ca ii, Ti ii and Zn ii. The individual 21-cm absorption components also have a similar velocities as the heavy metal absorption components. The 21-cm profile was found to vary on short timescales of a few days and models that reproduce the variable 21-cm absorption profile required small-scale variations of the optical depth of the absorber (Kanekar & Chengalur 2001a).

3.4 Galaxy Morphologies

In Figure 7 we show a zoomed-in contour plot of the galaxies in the field. The axes are set to the physical scale at the redshift of the DLA. The WFPC–2 F814W filter is comparable to the rest frame Kron-Cousins R filter at the $z = 0.313$ absorption redshift. Four of the galaxies in the $z = 0.313$ group are visible here along with both $z = 0.328$ galaxies. We plot surface brightness contours ranging be-

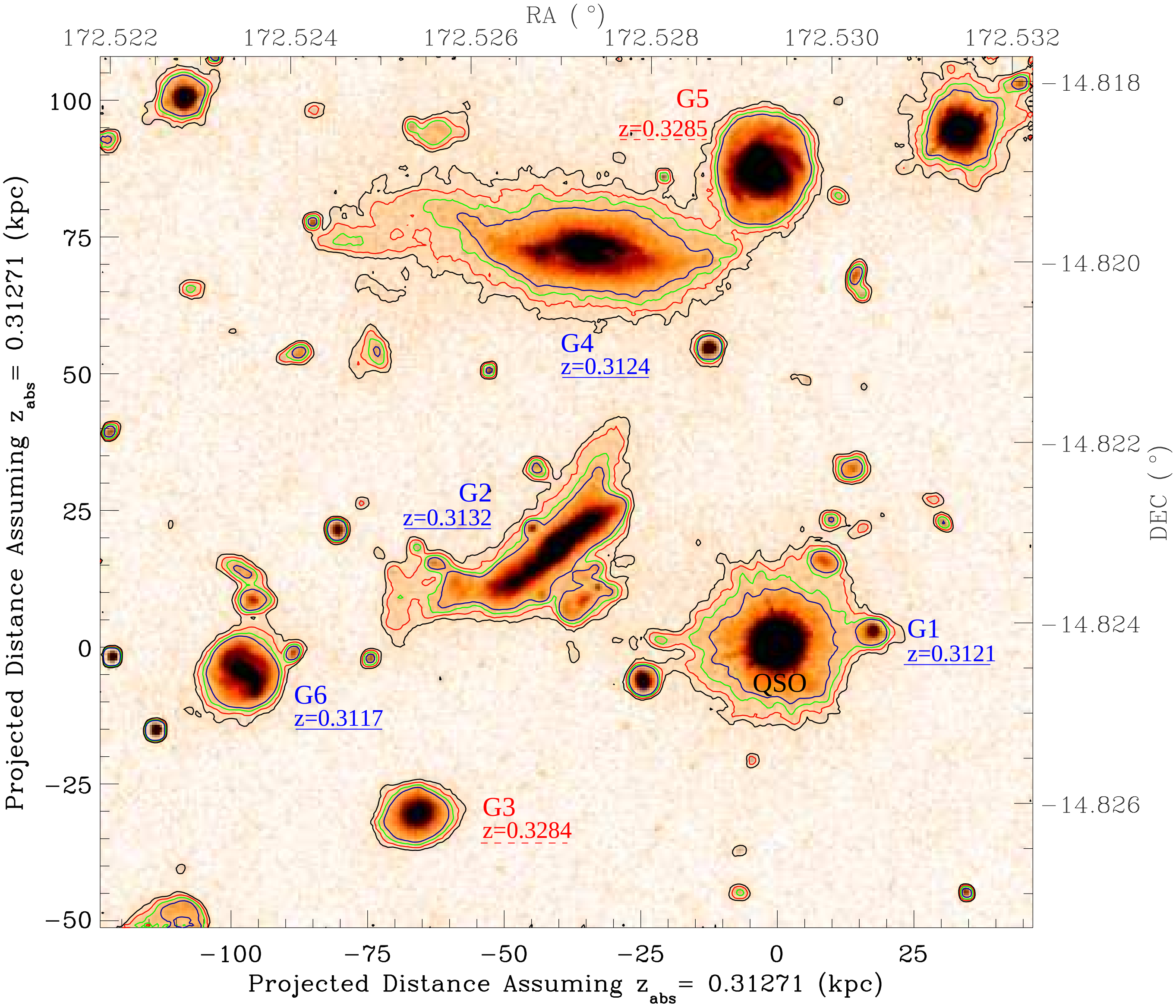

Figure 7. Smoothed surface brightness contour plot of the quasar field. The contours are in 0.3 mag arcsec^{-2} intervals: 23.3(blue), 23.6(green), 23.9(red), and 24.2(black) mag arcsec^{-2}. The surface brightness limit of the image is roughly 25 mag arcsec^{-2}. The axes indicate the projected distance away from the quasar in kpc (assuming $z = z_{abs} = 0.31271$) along with the RA and DEC in units of degrees. Note the extend optical streams - possibly tidal tails – seen for G2 and G4.

tween 23.3 – 24.2 mag arsec^{-2}. The image has a surface brightness limit of $\sim$ 25 mag arcsec^{-2}.

Upon inspecting the galaxies in the $z = 0.313$ group, one notices that both G2 and G4 seem to exhibit tidal disturbances. G2 contains either a strong warp in the disk or tidal tails from previous interactions. The rest-frame *R*-band optical streams extend up to 25 kpc away from the galaxy. These features suggest at least one merger/harassment event. The small galaxy situated below the semi-major axis of G2 in projection does not have a spectroscopic redshift. Using broad band photometry, Chen & Lanzetta (2003) derive a redshift of $z = 0.53$ for this faint object. However, if this object is undergoing an interaction with G2, then its colours may not be consistent with the standard spectral templates used to derive the photometric redshift. The redshift of this galaxy is in need of spectroscopic confirmation.

The S0-like galaxy G4, exhibits a strong dust lane and also has an extended optical stream extending ∼30 kpc projected in length towards the East from the galaxy center. This potential tidal stream is suggestive of previous interactions, possibly with G2. There are also several unidentified, large, low surface-brightness blobs above and below the stream, which may be associated with the tidal debris or high-redshift low surface brightness galaxies. The asymmetric spiral G6 may have some tidal debris as well since it has some optical structures in its vicinity but they could potentially be galaxies at different redshifts. The morphologies of the galaxies seen here suggest that this group has undergone some interactions in the past.

Table 4. The emission line rest frame equivalent widths and emission line fluxes for the absorbing galaxies. The [O II] equivalent width was not published by Lane et al. (1998). Only the Keck/ESI spectra of G5, G2, and G4 are flux calibrated.

		Rest Equivalent Width (Å)						Integrated Line Flux ($\times 10^{-18}$ erg s^{-1} cm^{-2})					
ID	z_{gal}	[O II]	Hβ	[O III]	[N II]	Hα	[N II]	[O II]	Hβ	[O III]	[N II]	Hα	[N II]
G3	0.32839	<5.1	···	···	<3.7	32.0±1.9	11.0±1.1	···	···	···	···	···	···
G5	0.32847	<2.0	<2.0	<1.2	7.4±1.8	29.5±2.3	22.1±2.3	<76	<43	<23	128±31	511±30	382±36
						$z_{abs} = 0.313$ Group							
G1	0.3121	···	···	···	···	···	···	···	···	···	···	···	···
G2	0.3132	5.8±0.5	<0.4	<0.4	2.7±0.4	17.3±1.3	9.0±0.8	99±8	<11	<12	95±15	602±33	295±28
G4	0.3124	2.4±1.0	<0.5	<0.6	<1.4	<1.5	<1.0	10±4	<7	<8	<31	<34	<23
G6	0.31167	<4.2	···	···	<2.9	32.4±1.9	11.1±1.1	···	···	···	···	···	···
G14	0.31243	···	···	···	<2.5	34.8±3.9	<5.1	···	···	···	···	···	···

It has been noted in the literature (Rao et al. 2003), and can be seen here, that there appears to be a significant level of surface brightness (SB) around the quasar. Rao et al. (2003) suggest that the low SB feature is potentially a low SB galaxy that is responsible for the DLA absorption. However, no evidence yet exists to support this possibility. It also remains possible that the emission seen in Figure 7 is associated with the $z_{em} = 1.18$ quasar host galaxy, which has extended radio and x-ray emission that overlap quite well with the extended quasar optical emission (see Siemiginowska et al. 2002, 2007). There are many faint galaxies/structures that remain unidentified in this field, several of which reside in close proximity to the quasar line of sight, that may also contribute to the absorption.

Our data suggest that most galaxies in the $z = 0.313$ group have undergone interactions in the past. One way to differentiate between these and the many possible origin scenarios for the DLA gas is by studying the galaxy star formation rates and by comparing the metallicity of the surrounding galaxies and of the absorption.

3.5 Metallicities and Star Formation Rates

In an effort to better understand the origins of the metal-enriched absorption, we compute, when possible, the galaxy star formation rates (SFRs) and metallicities.

We can only compute SFRs for galaxies that have Keck/ESI spectra which have been flux calibrated. The APO/DIS data were taken during poor/cloudy weather conditions and we are unable to flux calibrate them. We compute the galaxy SFRs using the Hα (Kewley et al. 2002) and [O II] (Kewley et al. 2004) emission line relations. We do not apply any dust corrections since we are unable to measure the Balmer decrement. We do not apply slit loss corrections. Thus, the SFRs quoted here are lower limits.

By contrast with the SFR calculations, we are able to compute metallicities for additional galaxies using only the equivalent widths of Hα and N II emission lines. Since both Hα and N II are only 20.66 Å (at rest wavelengths) apart, the continuum flux levels are approximately the same and are insensitive to dust reddening. Thus, the metallicity indicator $N2 = f(\text{N II}\lambda6583)/f(\text{H}\alpha)$, which is a ratio of emission line fluxes (f), becomes just the ratio of equivalent widths. This technique has been demonstrated to work for other metallicity indicators such as R_{23} (see Kobulnicky & Phillips 2003). We apply the $N2$ metallicity relation from Pettini & Pagel (2004), where 12+log(O/H)= $8.90 + 0.57 \times N2$. Note that the $N2$ metallicity indicator becomes unreliable above roughly solar since the $N2$ index saturates as nitrogen becomes the dominant coolant (see Erb et al. 2006, and references therein). We assume a solar oxygen abundance of $\log(\text{O/H})_\odot = 8.736 \pm 0.078$ (Holweger 2001). The star formation rates and metallicities are listed in Table 5.

For the $z = 0.313$ group we are able to measure star formation rates for galaxies G2 and G4. For G2 we compute SFR([O II])=0.44 M$_\odot$ yr^{-1} and SFR(Hα)=1.52 M$_\odot$ yr^{-1}. For G4 we compute SFR([O II])=0.045 M$_\odot$ yr^{-1}. Again, we have not applied any dust corrections which is probably the source of the difference between the SFRs derived from Hα and [O II]; the Hα SFR is more reliable since it is less affected by dust extinction than [O II]. Since the galaxy SFRs are not corrected for dust extinction, the SFRs quoted are lower limits. We note that both of these galaxies have typical SFRs and are not likely to have strong winds. Even if dust corrections were applied, it would at most increase the SFRs by a factor of ~ 2 which is still lower than expected for galaxies with strong winds. The S0-like morphology of G4 is consistent with low SFRs and no strong outflow winds. Given that G2 and G4 are the brightest galaxy group members closest to the quasar LOS, it is unlikely that the absorption is coming from winds. We can compute the metallicities for three of the galaxies in the group: [O/H]= 0.00 ± 0.09 for G2, [O/H]= -0.10 ± 0.09 for G6, and a limit of [O/H]< -0.31 for G14. These galaxies are roughly solar in abundance except for G14 which is less than 1/2 solar.

The DLA absorption metallicity was initially derived from the amount of photoelectric absorption due to metals present in the quasar X-ray spectrum. The derived metallicity ranged from zero to solar (Bechtold et al. 2001; Turnshek et al. 2003). Although, zero metallicity is unlikely due to the observed metal lines in absorption (Figure 6), it can only be concluded that there is no evidence for a relatively high metallicity DLA (Turnshek et al. 2003). Kanekar et al. (2009) used STIS E230M quasar spectra to compute the absorption metallicity using the Zn II λ2026 and λ2062 lines. Zn abundance measurements give metallicity estimates relatively free of depletion effects since Zn is relatively undepleted on to dust grains. Kanekar et al. (2009) compute a metallicity of the $z_{abs} = 0.313$ DLA to be [Zn/H]= -0.90 ± 0.11 relative to solar.

To compare the metallicity of this DLA to the general population of DLAs, we use the work of Kulkarni et al. (2005) who computed the N(H I)-weighted mean [Zn/H] metallicity for 20 DLAs between $0.09 < z < 1.37$. They derived a mean [Zn/H]= -0.86 ± 0.11 for their maximum-limits sample, [Zn/H]= -1.01 ± 0.14 for their minimum-limits sample. The maximum-limits sample treats the Zn limits as detections and the minimum-limits sample treats the Zn limits as zeros. The Q1127−145 $z = 0.313$ DLA has roughly typical metallicity.

Table 5. Star formation rates and metallicities for galaxies associated with the z_{abs} = 0.328266 and the z_{abs} = 0.312710 DLA. The galaxy star formation rates are not corrected for host galaxy dust extinction and the SFRs quoted are lower limits. However, even with applying such correction, the SFRs would not be strong enough to produce strong large-scale galactic winds. The errors in the metallicities include the statistical errors of the measurement of the emission line equivalent width measurements, fits to the continuum, and the errors in the empirical metallicity calibrators used.

Galaxy	SFR([O ii]) $\mathrm{M}_\odot\,\mathrm{yr}^{-1}$	SFR(Hα) $\mathrm{M}_\odot\,\mathrm{yr}^{-1}$	12+log(O/H)	[O/H]^b
G3	···	···	8.64±0.05	−0.10±0.09
G5	···	1.44	8.83±0.06	0.09±0.1
z_{abs} = 0.313 Group				
G1	···	···	···	···
G2	0.44	1.52	8.74±0.05	0.00±0.09
G4	0.045	···	···	···
G6	···	···	8.64±0.05	−0.10±0.09
G14	···	···	<8.43	< −0.31

^{b}Here [X/Y]=log(X/Y)−log(X/Y)$_\odot$.

To summarize the metallicity comparison, we find that the gas in absorption is relatively metal poor compared to the galaxies for which we could compute metallicities. We obtain roughly solar metallicity for the galaxies and 1/10th solar for the absorption system.

For the $z = 0.328$ galaxy pair, we compute the SFR for G5 using the Hα emission lines resulting in a SFR(Hα)= 1.44 $\mathrm{M}_\odot\,\mathrm{yr}^{-1}$. The galaxy has a SFR much lower than would be expected for strong outflows (Weiner et al. 2009). We are able to measure the metallicities for both galaxies (G3 and G5) associated with the $z = 0.328$ absorption. G3 has a [O/H]= −0.10 ± 0.09 and G5 has a [O/H]= 0.09 ± 0.1. That is, the galaxies have similar metallicity which is approximately solar. Unfortunately, since the absorption system is quite weak, we cannot measure an absorption metallicity for this system for direct comparison. Furthermore, from the *HST*/FOS G160L quasar spectrum (see Rao & Turnshek 2000) it is apparent that the $z = 0.328$ Lyα absorption is embedded within the z_{abs} = 0.312710 DLA Lyα absorption and cannot be deblended.

4 DISCUSSION

4.1 z_{abs} = 0.313 Galaxies

In most circumstances, DLAs are produced from quasar lines of sight passing either through or near isolated galaxies (e.g., Lacy et al. 2003; Møller et al. 2002; Rao et al. 2003; Chun et al. 2006). However, in the case of the $z = 0.313$ DLA, the environment is more complex. Here we find a group of galaxies associated with the DLA system containing at least five members with a velocity dispersion $\sigma = 115$ km s^{-1} offset 80 km s^{-1} blueward of the Mg ii absorption redshift. The DLA associated with the $z = 0.313$ group has $W_r(2796) = 1.773$ Å. The group as a luminosity range of $0.04 \leqslant L_B \leqslant 0.63 L_B^\star$ and an impact parameter range of $17.4 \leqslant D \leqslant 240.8$ kpc. The galaxy redshift distribution is consistent with the Mg ii absorption velocity distribution, along with the other metals. Furthermore, measured projected rotation curves of two of the galaxies (G2 and G4) also cover the entire absorption velocity range.

From the derived galaxy emission line metallicities and the DLA absorption metallicity, at first it appears unlikely that the absorption is produced by metal-enriched winds or tidal debris from these two galaxies. Recent metallicity gradient measurements, derived from local early type galaxies, have been shown to be quite shallow and extend for several galaxy effective radii; Spolaor et al. (2010) find an average stellar absorption metallicity gradient of −0.22 ± 0.14 per effective radius for their sample. G2 has an effect radius of 8.1 ± 0.6 kpc (Kacprzak et al. 2007) which, with this metallicity gradient, would imply that the metallicity at the quasar line of sight would be [O/H]= −1.2 ± 0.7. Although the errors are large, this is consistent with the absorption system metallicity observed. This result is similar for G6. Thus, it is possible that the absorption is produced by an extended disk that has a shallow metallicity gradient. However, it has not been demonstrated that these metallicity gradients can be smoothly extrapolated beyond a few disk effective radii into the halo.

The only other direct comparison of galaxy emission line and quasar absorption line metallicity was by Bowen et al. (2005) at redshift $z = 0.009$. The DLA has an impact parameter of 3.3 kpc from the absorbing dwarf galaxy and the galaxy and the DLA have very similar metallicities, perhaps implying a relatively flat radial abundance gradient. This makes it difficult to determine if the gas originates in the galaxy disk or outflows. Chen et al. (2005) attempted to compare host galaxy/absorber metallicities for three systems and found that the galaxy metallicity derived from [O/H] greater than the absorption metallicity derived from [Fe/H]. They proposed radial metallicity gradients to explain their results. However, these results remain uncertain because the absorption metallicities were derived using iron, which has variable degree of dust depletion. Undepleted elements such as Zn provide much more robust metallicity estimates which can be more reliably compared to [O/H] metallicities derived for galaxies.

The outflow scenario is supported by Bouché et al. (2006) who found a statistical anti-correlation between Mg ii absorption-line equivalent width and the mass of the halo hosting the absorbers by cross-correlating absorbers with luminous red galaxies in the SDSS. They claim that this is direct evidence that absorbers are not virialized in gaseous halos of the galaxies. They suggest that the strongest absorbers – those with $W_r(2796) \gtrsim 2$ Å, somewhat stronger than the one associated with the $z = 0.313$ group – are statistically more likely to trace super-winds.

Strong winds can be seen directly in absorption. For example, stacking 1400 DEEP2 galaxy spectra at z~1.4, Weiner et al. (2009) found 300–1000 km/s winds in Mg ii and Mg i absorption in galaxies with high SFRs and that both Mg ii equivalent width and the outflow velocities are correlated with galaxy SFRs. At lower redshifts (z~0.6), Tremonti et al. (2007) reported Mg ii absorption blueshifted 500–2000 km/s relative to 14 post-starburst host galaxies. Although some of these systems may not be DLAs, Rao et al. (2006) showed that ~35% of (MgII-selected) absorbers with Mg iiλ2796 and Fe iiλ2600 > 0.5 Å are DLAs. We find low SFRs in the two brightest galaxy members of the $z = 0.313$ group (G2 and G4) and would not expect to see strong winds as discussed above. However, we do not have SFR estimates for galaxy G1 which is at the closet projected distance to the quasar line of sight. If this faint galaxy has/had high SFRs, then according to the Bouché et al. (2006) results, this galaxy may have a high probability of being a major contributor to the Mg ii absorption. If the gas was traveling at moderate wind speeds of 100 km s^{-1} then it would only take ∼ 0.2 Gyr to reach the quasar line of sight from G1. Though this is a plausible argument, the tidal features seen for galaxies G2 and G4 suggest a different story.

This is not the first group discovered to be associated with Mg II absorption. Whiting et al. (2006) detected a group of five galaxies ($z = 0.66$) with a velocity dispersion of $\sigma = 430$ km s^{-1} associated with a Mg II absorption system with a velocity width of 250 km s^{-1}. Four of the five galaxies have impact parameters less than 100 kpc with the smallest at 51.2 kpc. They report that it is difficult to associate a given galaxy to the absorption system and that debris produced by interactions may be producing the absorption. DLAs originating from tidal gas in galaxy groups are further supported by Nestor et al. (2007) who found that very strong Mg II absorbers often arise in fields with multiple galaxies in close proximity to the quasar LOS. They do not have galaxy redshifts in the quasar fields, yet they argue that the likely origin of the high equivalent width Mg II absorption is kinematically disturbed gas around interacting galaxies. However, both studies used only ground based imaging and were not able to directly study the morphologies of the group members.

For the $z_{abs} = 0.313$ galaxy group, two of the brightest members (G2, G4, and possibly G6) exhibit perturbed morphologies and several extended optical streams. These streams extend for $\sim$ 25 kpc and may reflect the recent merger/interaction history of this galaxy group; they may comprise tidal debris. The interactions producing the tidal debris seen here may also be responsible for producing the complex absorption system. The absorption could arise directly from the tidal debris or from dwarf galaxies that form in these tidal tails (Knierman et al. 2003).

Physical properties of the DLA absorbing gas are further constrained by Kanekar et al. (2009) who derived a 21-cm gas covering fraction of 0.9 and a gas spin temperature of $T_s = 820 \pm 145$ K. Spin temperatures of $T_s \sim 300$ K are typical for local spiral galaxies and the Milky Way. Higher spin temperatures are associated with smaller objects such as dwarf galaxies, low surface brightness galaxies, or objects with low metallicity/pressure that have a larger fraction of warm gas and where physical conditions are not suitable for producing the cold phase of HI (Wolfire et al. 1995). However, the majority of DLAs (including the $z_{abs} = 0.313$ DLA) have far higher spin temperatures: $T_s > 500$ K (Carilli et al. 1996; Kanekar et al. 2009). It has been debated that the high temperature estimates for DLAs may arise due to the difference between radio and optical gas covering fractions (Curran et al. 2005) and/or wavelength dependent beam size or sightline (Wolfe et al. 2003). Although these effects may play a role, a recently reported correlation between DLA [Z/H] and T_s may suggest that there is no wavelength dependence on the observations (Kanekar et al. 2009). Given the large extended structure observed in the radio for the Q1127−145 quasar, including the radio jet, it is possible this system may suffer from such wavelength dependent effect, thereby making it difficult to compare optical and 21-cm absorption data. It has been mentioned in the literature that quasar Q1127−145 is a peculiar case, since it has a rather large 21-cm absorption profile velocity width and a high spin temperature (Kanekar & Chengalur 2001b), suggesting that this system is different from standard DLAs. Thus, it is plausible that the both the optical and 21-cm absorption may arise in structures such as tidal streams, infall and/or outflows.

The full velocity range of 350 km s^{-1} for the Mg II absorption profiles (along with Fe II) remain difficult to reproduce in kinematic models. The cloud velocity distribution simulations of Prochaska & Wolfe (1997) suggest that DLA velocity profiles are driven by rapidly-rotating thick disks. Also, 21-cm observations of low-mass galaxies, such as the Large Magellanic Cloud, display lower velocity widths than observed for typical DLAs (Prochaska et al. 2002). This supports the idea that DLAs are massive rotating extended disks of galaxies. However, hydrodynamical simulations of Haehnelt et al. (1998) showed that irregular protogalactic clumps can reproduce the DLA absorption-line velocity width distribution equally well. They conclude that the absorption velocity widths can be driven by a variety of structures, which are a superposition of rotation, random motions, infall, and merging. Additional 21-cm studies of Zwaan et al. (2008) demonstrated that the DLA velocity widths do not originate from rotating gas disks of galaxies similar to those seen in the local universe. These results further support that DLAs are often associated with tidal gas produced by galaxy interactions or superwinds and outflows.

Given the data we have acquired, and the arguments that we have presented, we favor the interpretation that the DLA absorption arises from tidal debris produced by galaxy interactions, which are likely more important in the $z = 0.313$ group environment we have identified. However, we cannot completely rule out other scenarios such as outflows originating from the galaxy group members, faint unidentified galaxies near the quasar LOS, or small satellite galaxies in front of the quasar LOS.

4.2 $z_{abs} = 0.328$ Galaxies

The $z = 0.328$ pair of galaxies is associated with a weak Mg II absorption system. Both galaxies, G3 and G5, are within the fiducial Mg II halo size of ~100 kpc. G5 is roughly 2.5 times more luminous than G3. Both galaxies have velocities that are consistent with the absorption velocities (see Figure 4), which makes it difficult to associate one particular galaxy to the absorption system. The SFR of G5 is typical of a normal spiral galaxy and would not be expected to have strong outflows (e.g., Heckman 2002, 2003; Weiner et al. 2009).

Both galaxies have similar metallicities which are roughly solar. Even if we had the metallicity of the absorption system we would not be able to identify the host galaxy. For reference, Narayanan et al. (2008) analyzed 100 weak Mg II absorbers and found, using ionization modeling, that the metallicity in a significant fraction of systems are constrained to values of solar or higher. If this was true for this particular case, both galaxies would be in agreement with the absorption metallicity. There is no clear evidence of strong disruptions in the morphology of either galaxy, indicating no recent merger or interaction activity. Given that the absorption system is very weak, it could arise in a wide array of structures associated with the environment of the pair of galaxies.

5 CONCLUSIONS

We have performed a spectroscopic galaxy survey to limiting magnitude of $m_{F814W} \leqslant 20.3$ ($L_B > 0.15L_*$ at $z = 0.3$) within $100{\times}100''$ of the quasar Q1127−145. This field has a large number of bright galaxies near the quasar line of sight and has three Mg II absorption systems detected in the quasar spectrum, including one DLA. Here we have obtained spectroscopic redshifts for eight galaxies in this field, adding to the four previously identified (Bergeron & Boissé 1991; Guillemin & Bergeron 1997; Kacprzak et al. 2010).

Our main results can be summarized as follows:

(i) We have identified two galaxies (G6 and G14) associated with the DLA at $z = 0.313$, which, in addition to the three known galaxies, form a group of at least five galaxies. The group has a luminosity range of $0.04 \leqslant L_B \leqslant 0.63L_B^\star$ and an impact parameter range of $17.4 \leqslant D \leqslant 240.8$ kpc. The group velocity dispersion is

$\sigma = 115$ km s^{-1} having a full velocity range of ~ 350 km s^{-1}. The group redshift is offset 80 km s^{-1} blueward of the Mg II absorption redshift. The galaxy redshift distribution spans the entire range of the absorption velocities. Furthermore, the rotation curves of G2 and G4 alone cover the entire range of absorption velocities.

Star formation rates of two of the brightest galaxy members are too low to drive strong winds, reducing the likelihood that winds are responsible for the absorbing gas. Metal enriched winds are also unlikely since the DLA metallicity is 1/10th solar, whereas three of the five galaxies have metallicities range between less than 1/2 solar to solar. Although stellar metallicity gradients in the literature are consistent with our findings, it is has yet to be demonstrated that these gradients can be extrapolated to 50 kpc. The favored scenario for the origin of the absorption is from tidal debris. The deep WFPC–2 F814W imaging shows the perturbed morphologies for three galaxies and optical tidal tails extending ~ 25 kpc away from the disks. These features suggest merger/harassment events, consistent with the more frequent galaxy harassment/merging expected in the group environment we have identified.

(ii) We have identified a galaxy (G3), in addition to previously identified G5 (Kacprzak et al. 2010), associated with the $z = 0.328$ weak Mg II absorption system, $W_r(2796) = 0.029$ Å. There is no evidence of recent interactions since both galaxies have unperturbed morphologies and they are separated by 140 kpc. Even armed with the star-formation rate and rotation velocities of G5 and the metallicities of both galaxies, it remains difficult to determine which galaxy hosts the absorber. We can only conclude that this weak absorption system can arise in a variety of cosmic structures in either or both halos of the galaxy pair.

(iii) We have identified five galaxies (G7, G9, G11, G12, and G15) with $0.21 \leqslant z \leqslant 0.33$ that are not associated with any detectable Mg II absorption (3σ detection limits of 4.8 – 5.7 mÅ). These galaxies appear to be normal star-forming spiral disks. All non-absorbing galaxies have impact parameters $D > 118$ kpc. This is consistent with previous results on Mg II halo sizes, which suggest we should not expect to detect absorption beyond impact parameters of ~ 120 kpc.

The DLA-galaxy group at $z = 0.313$ is quite different from the standard examples in literature of DLA-plus-(apparently) isolated galaxy (e.g., Lacy et al. 2003; Møller et al. 2002; Rao et al. 2003; Chun et al. 2006). The group of galaxies associated with the $z = 0.313$ DLA suggests that interactions, which are common in groups of galaxies, might be responsible for at least some DLA absorption systems as well. This may explain why searches for host galaxies of DLAs and strong Mg II systems have a low success rate of 30–40% using small field of view IFUs (e.g., Bouché et al. 2007). It is likely that we need to survey further out from the quasar line of sight if there are many other cases where tidal debris produces the absorption. It is also interesting to note that if this galaxy group was at a slightly higher redshift, we would not be able to detect the $0.04L_B^{\star}$ galaxy that is closest to the quasar line of sight, which could even be the DLA host. Given the low redshift of the DLA and even using the deep *HST* imaging, star formation rates, and metallicities, it is difficult to understand this complex system and determine the origins of the absorbing gas. We emphasize that we should take caution in concluding the origins of absorbing gas drawn from studies of individual DLAs at higher redshifts.

ACKNOWLEDGMENTS

We thank Frank Briggs for his useful comments and for carefully reading this paper. We thank Greg Wirth for his help and advice with ESI/Keck. MTM thanks the Australian Research Council for a QEII Research Fellowship (DP0877998). CWC was supported by the National Science Foundation under Grant Number AST-0708210. This work is based on observations obtained with the Apache Point Observatory 3.5-meter telescope, which is owned and operated by the Astrophysical Research Consortium. Observations were also made with the NASA/ESA *Hubble Space Telescope*, or obtained from the data archive at the Space Telescope Institute. Other observations were made with the ESO Very Large Telescope at the Paranal Observatories. Based on observations made with the NASA/ESA Hubble Space Telescope, and obtained from the Hubble Legacy Archive, which is a collaboration between the Space Telescope Science Institute (STScI/NASA), the Space Telescope European Coordinating Facility (ST-ECF/ESA) and the Canadian Astronomy Data Centre (CADC/NRC/CSA). Some of the data presented herein were obtained at the W.M. Keck Observatory, which is operated as a scientific partnership among the California Institute of Technology, the University of California and the National Aeronautics and Space Administration. The Observatory was made possible by the generous financial support of the W.M. Keck Foundation.

REFERENCES

Barton, E. J., & Cooke, J. 2009, AJ, 138, 1817

Bechtold, J., Siemiginowska, A., Aldcroft, T. L., Elvis, M., & Dobrzycki, A. 2001, ApJ, 562, 133

Bergeron, J. 1986, A&A, 155, L8

Bergeron, J. 1988, Large Scale Structures of the Universe, 130, 343

Bergeron, J., & Boissé, P. 1991, A&A, 243, 334

Bertin, E., & Arnouts, S. 1996, A&AS, 117, 393

Bouché, N., Murphy, M. T., Péroux, C., Csabai, I. & Wild. V. 2006 MNRAS, 371, 495

Bouché, N., Murphy, M. T., Péroux, C., Davies, R., Eisenhauer, F., Förster Schreiber, N. M., & Tacconi, L. 2007, ApJL, 669, L5

Bowen, D. V., Jenkins, E. B., Pettini, M., & Tripp, T. M. 2005, ApJ, 635, 880

Burkert, A., & Lin, D. N. C. 2000, ApJ, 537, 270

Carilli, C. L., Lane, W., de Bruyn, A. G., Braun, R., & Miley, G. K. 1996, AJ, 111, 1830

Chelouche, D., Ménard, B., Bowen, D. V., & Gnat, O. 2008, ApJ, 683, 55

Chen, H.-W., Kennicutt, R. C., Jr., & Rauch, M. 2005, ApJ, 620, 703

Chen, H.-W. & Lanzetta, K. M. 2003, ApJ, 597, 706

Chen, H.-W., & Tinker, J. L. 2008, ApJ, 687, 745

Chengalur, J. N., & Kanekar, N. 2000, MNRAS, 318, 303

Chun, M. R., Gharanfoli, S., Kulkarni, V. P., & Takamiya, M. 2006, AJ, 131, 686

Churchill, C. W., Kacprzak, G. G., & Steidel, C. C. 2005, in *Probing Galaxies through Quasar Absorption Lines*, IAU 199 Proceedings, eds. P. R. Williams, C.–G. Shu, & B. Ménard (Cambridge: Cambridge University Press), p. 24

Churchill, C. W., Mellon, R. R., Charlton, J. C., Jannuzi, B. T., Kirhakos, S., Steidel, C. C., & Schneider, D. P. 2000a, ApJS, 130, 91

Churchill, C. W., Mellon, R. R., Charlton, J. C., Jannuzi, B. T., Kirhakos, S., Steidel, C. C., & Schneider, D. P. 2000b, ApJ, 543, 577

Churchill, C. W., Rigby, J. R., Charlton, J. C., & Vogt, S. S. 1999, ApJS, 120, 51

Churchill, C. W., Steidel, C. C., & Vogt, S. S. 1996, ApJ, 471, 164

Churchill, C. W., & Vogt, S. S. 2001, AJ, 122, 679

Curran, S. J., Murphy, M. T., Pihlström, Y. M., Webb, J. K., & Purcell, C. R. 2005, MNRAS, 356, 1509

Chynoweth, K. M., Langston, G. I., Yun, M. S., Lockman, F. J., Rubin, K. H. R., & Scoles, S. A. 2008, AJ, 135, 1983

Dekker, H., D'Odorico, S., Kaufer, A. Delabre, B. & Kotzlowski H. 2000, SPIE, 4008, 534

Ellison, S. L., Mallén-Ornelas, G., & Sawicki, M. 2003, ApJ, 589, 709

Erb, D. K., Steidel, C. C., Shapley, A. E., Pettini, M., Reddy, N. A., & Adelberger, K. L. 2006, ApJ, 646, 107

Faber, S. M., et al. 2007, ApJ, 665, 265

Fraternali, F., van Moorsel, G., Sancisi, R., & Oosterloo, T. 2002, AJ, 123, 312

Guillemin p., & Bergeron, J. 1997, A&A, 328, 499

Haehnelt, M. G., Steinmetz, M., & Rauch, M. 1998, ApJ, 495, 647

Heckman, T. M. 2002, Extragalactic Gas at Low Redshift, 254, 292

Heckman, T. M. 2003, Revista Mexicana de Astronomia y Astrofisica Conference Series, 17, 47

Holweger, H. 2001, Joint SOHO/ACE workshop "Solar and Galactic Composition", 598, 23

Kacprzak, G. G., Churchill, C. W., Steidel, C. C., & Murphy, M. T. 2008, AJ, 135, 922

Kacprzak, G. G., Churchill, C. W., Steidel, C. C., Murphy, M. T., & Evans, J. L 2007, ApJ, 662, 909

Kacprzak, G. G., Churchill, C. W., Ceverino, D., Steidel, C. C., Klypin, A., & Murphy, M. T. 2010, ApJ, 711, 533

Kanekar, N., & Chengalur, J. N. 2001b, A&A, 369, 42

Kanekar, N., & Chengalur, J. N. 2001a, MNRAS, 325, 631

Kanekar, N., Smette, A., Briggs, F. H., & Chengalur, J. N. 2009, ApJl, 705, L40

Kaufmann, T., Bullock, J. S., Maller, A. H., Fang, T., & Wadsley, J. 2009, MNRAS, 396, 191

Kewley, L. J., Geller, M. J., & Jansen, R. A. 2004, AJ, 127, 2002

Kewley, L. J., Geller, M. J., Jansen, R. A., & Dopita, M. A. 2002, AJ, 124, 3135

Kim, A., Goobar, A., & Perlmutter, S. 1996, PASP, 108, 190

Kinney, A. L., Calzetti, D., Bohlin, R. C., McQuade, K., Storchi–Bergmann, T. & Schmitt, H. R. 1996, ApJ, 467, 38

Knierman, K. A., Gallagher, S. C., Charlton, J. C., Hunsberger, S. D., Whitmore, B., Kundu, A., Hibbard, J. E., & Zaritsky, D. 2003, AJ, 126, 1227

Kobulnicky, H. A., & Phillips, A. C. 2003, ApJ, 599, 1031

Kulkarni, V. P., Fall, S. M., Lauroesch, J. T., York, D. G., Welty, D. E., Khare, P., & Truran, J. W. 2005, ApJ, 618, 68

Lacy, M., Becker, R. H., Storrie-Lombardi, L. J., Gregg, M. D., Urrutia, T., & White, R. L. 2003, AJ, 126, 2230

Lane, W., Smette, A., Briggs, F., Rao, S., Turnshek, D., & Meylan, G. 1998, AJ, 116, 26

Lanzetta, K. M., & Bowen, D. 1990, ApJ, 357, 321

Lanzetta, K. M. & Bowen, D. V. 1992, ApJ, 391, 48L

Le Brun, V., Bergeron, J., Boisse, P., & Christian, C. 1993, A&A, 279, 33

Lin, D. N. C., & Murray, S. D. 2000, ApJ, 540, 170

Lopez, S., et al. 2008, ApJ, 679, 1144

Maller, A. H., & Bullock, J. S. 2004, MNRAS, 355, 694

Matteucci, F., Molaro, P., & Vladilo, G. 1997, A&A, 321, 45

Ménard, B., Wild, V., Nestor, D., Quider, A., & Zibetti, S. 2009, arXiv:0912.3263

Mo, H. J., & Miralda-Escude, J. 1996, ApJ, 469, 589

Møller, P., Warren, S. J., Fall, S. M., Fynbo, J. U., & Jakobsen, P. 2002, ApJ, 574, 51

Mulchaey, J. S., & Zabludoff, A. I. 1998, ApJ, 496, 73

Narayanan, A., Misawa, T., Charlton, J. C., & Kim, T.-S. 2007, ApJ, 660, 1093

Narayanan, A., Charlton, J. C., Misawa, T., Green, R. E., & Kim, T.-S. 2008, ApJ, 689, 782

Nestor, D. B., Rao, S. M., Turnshek, D. A., Monier, E., Lane, W. M., & Bergeron, J. 2002, Extragalactic Gas at Low Redshift, 254, 34

Nestor, D. B., Turnshek, D. A., Rao, S. M., & Quider, A. M. 2007, ApJ, 658, 185

Padilla, N., Lacerna, I., Lopez, S., Barrientos, L. F., Lira, P., Andrews, H., & Tejos, N. 2009, MNRAS, 395, 1135

Pettini, M., & Pagel, B. E. J. 2004, MNRAS, 348, L59

Pollack, L. K., Chen, H.-W., Prochaska, J. X., & Bloom, J. S. 2009, ApJ, 701, 1605

Prochaska, J. X., Ryan-Weber, E., & Staveley-Smith, L. 2002, PASP, 114, 1197

Prochaska, J. X., & Wolfe, A. M. 1998, ApJ, 507, 113

Prochaska, J. X., & Wolfe, A. M. 1997, ApJ, 487, 73

Puche, D., Westpfahl, D., Brinks, E., & Roy, J. 1992, AJ, 103, 1841

Rand, R. 2000, ApJ, 537, 13

Rao, S. M., Turnshek, D. A., & Nestor, D. B. 2006, ApJ, 636, 610

Rao, S. M., Nestor, D. B., Turnshek, D. A., Lane, W. M., Monier, E. M., & Bergeron, J. 2003, ApJ, 595, 94

Rao, S. M., & Turnshek, D. A. 2000, ApJS, 130, 1

Rigby, J. R., Charlton, J. C., & Churchill, C. W. 2002, ApJ, 565, 743

Rubin, K. H. R., Prochaska, J. X., Koo, D. C., Phillips, A. C., & Weiner, B. J. 2009a, arXiv:0907.0231

Rubin, K. H. R., Weiner, B. J., Koo, D. C., Martin, C. L., Prochaska, J. X., Coil, A. L., & Newman, J. A. 2009b, arXiv:0912.2343

Sancisi, R., Fraternali, F., Oosterloo, T., & van der Hulst, T. 2008, A&A Rev., 15, 189

Siemiginowska, A., Bechtold, J., Aldcroft, T. L., Elvis, M., Harris, D. E., & Dobrzycki, A. 2002, ApJ, 570, 543

Siemiginowska, A., Stawarz, Ł., Cheung, C. C., Harris, D. E., Sikora, M., Aldcroft, T. L., & Bechtold, J. 2007, ApJ, 657, 145

Spolaor, M., Kobayashi, C., Forbes, D. A., Couch, W. J., & Hau, G. T. 2010, MNRAS, submitted

Steidel, C. C., Kollmeier, J. A., Shapely, A. E., Churchill, C. W., Dickinson, M., & Pettini, M. 2002, ApJ, 570, 526

Steidel, C. C., Dickinson, M., Meyer, D. M., Adelberger, K. L., & Sembach, K. R. 1997, ApJ, 480, 586

Steidel, C. C., Dickinson, M., & Persson, S. E. 1994, ApJ, 437, L75

Steidel, C. C., & Sargent, W. L. W. 1992, ApJs, 80, 1

Swaters, R. A., Sancisi, R., & van der Hulst, J. M. 1997, ApJ, 491, 140

Tinker, J. L., & Chen, H.-W. 2008, ApJ, 679, 1218

Tremonti, C. A., Moustakas, J., & Diamond-Stanic, A. M. 2007, ApJL, 663, L77

Turnshek, D. A., Rao, S. M., Ptak, A. F., Griffiths, R. E., & Monier, E. M. 2003, ApJ, 590, 730

Weiner, B. J., et al. 2009, ApJ, 692, 187

Wolfe, A. M., Gawiser, E., & Prochaska, J. X. 2003, ApJ, 593, 235

Wolfe, A. M., Turnshek, D. A., Smith, H. E., & Cohen, R. D. 1986, ApJS, 61, 249

Wolfire, M. G., Hollenbach, D., McKee, C. F., Tielens, A. G. G. M., & Bakes, E. L. O. 1995, ApJ, 443, 152

Whiting, M. T., Webster, R. L., & Francis, P. J. 2006, MNRAS, 368, 341

York, D. G., Dopita, M., Green, R., & Bechtold, J. 1986, ApJ, 311, 610

Zibetti, S., Ménard, B., Nestor, D. B., Quider, A. M., Rao, S. M., & Turnshek, D. A. 2007, ApJ, 658, 161

Zabludoff, A. I., & Mulchaey, J. S. 1998, ApJ, 496, 39

Zwaan, M., Walter, F., Ryan-Weber, E., Brinks, E., de Blok, W. J. G., & Kennicutt, R. C. 2008, AJ, 136, 2886